



Temperature measurement error reduction for MRI-guided HIFU treatment

Xiaodong Zhou, Qiang He, Al Zhang, Marc Beckmann & Cheng Ni

To cite this article: Xiaodong Zhou, Qiang He, Al Zhang, Marc Beckmann & Cheng Ni (2010) Temperature measurement error reduction for MRI-guided HIFU treatment, International Journal of Hyperthermia, 26:4, 347-358, DOI: [10.3109/02656731003601737](https://doi.org/10.3109/02656731003601737)

To link to this article: <https://doi.org/10.3109/02656731003601737>



Published online: 08 Apr 2010.



Submit your article to this journal [↗](#)



Article views: 513



View related articles [↗](#)



Citing articles: 1 View citing articles [↗](#)

Temperature measurement error reduction for MRI-guided HIFU treatment

XIAODONG ZHOU^{1,2}, QIANG HE^{1,2}, AL ZHANG², MARC BECKMANN², & CHENG NI^{1,2}

¹College of Life Science and Technology, Tongji University, Shanghai China and ²Siemens Mindit Magnetic Resonance Ltd, Shenzhen, China

(Received 18 February 2009; Revised 7 December 2009; Accepted 6 January 2010)

Abstract

Purpose: We present a method to remove the temperature measurement errors due to the movement of the ultrasound applicator during MRI-guided high-intensity focused ultrasound (MRgHIFU) treatment.

Methods: MR thermometry, based on proton resonance frequency (PRF) shift, can provide high accuracy and temporal resolution of MR temperature imaging for tumour treatment by MRgHIFU. However, the challenge is that the movement of the ultrasound applicator causes temperature measurement errors due to the magnetic susceptibility of the applicator. In a clinical environment the applicator has to be moved to cover the whole tumour volume, even in the case of a phased array ultrasound applicator. With conventional PRF shift-based phase mapping method, a reference image must be repetitively acquired as the ultrasound applicator is repositioned and tissue cooling down time must be inserted before a new reference scan. Therefore, the treatment workflow becomes complex and time consuming. In this paper we propose a method to reduce temperature measurement error by compensating the ultrasound applicator susceptibility through a pre-measured or calculated magnetic field distribution of the applicator.

Results: The large temperature measurement error shown around the ultrasound focal region can be significantly reduced by compensating the ultrasound applicator-induced delta magnetic field. Accurate temperature maps can be obtained when the ultrasound applicator is repositioned without repetitively acquiring new reference images.

Conclusions: The reference image can be repetitively used for the temperature imaging when the ultrasound applicator is repositioned. Therefore, the treatment workflow is simplified resulting in a reduction in total treatment time.

Keywords: MR thermometry, focused ultrasound, susceptibility, HIFU

Introduction

In recent years, magnetic resonance imaging (MRI)-guided high intensity focused ultrasound (MRgHIFU) treatment has been employed clinically in the treatment of uterine fibroids and has been approved by the US Food and Drug Administration (FDA). Treatments of other body organs such as liver, bone, breast, prostate and head have been reported by many researchers [1–9]. The advantage

of employing MRI is that it can provide real-time thermal dose monitoring as well as anatomical images during treatment [10]. It also provides contrast-enhanced images for evaluating treatment effectiveness after the treatment [11]. MR thermometry can provide temperature information that indicates the ‘thermal dose’ delivered to a tumour. This thermal dose is one of the most important factors to influence the efficacy of the treatment.

It measures the time integral over an exponential function of temperature and expresses as equivalent minutes at a reference temperature of 43°C [12]. When thermal dose reaches the 240 equivalent minutes threshold, the tumour tissue can be completely necrosed [13, 14]. Therefore, MRgHIFU can increase the effectiveness of HIFU treatment and reduce the treatment time, avoiding insufficient treatment as well as over treatment.

Among several MR thermometry methods, the PRF shift-based phase mapping method can provide high temperature accuracy and temporal resolution [15]. The relationship between proton resonance frequency and temperature was discovered by Hindman when he studied molecular interaction [16]. Ishihara [17] first applied the PRF shift-based method to magnetic resonance imaging. Due to its high imaging speed and temperature accuracy, the PRF shift-based MR temperature imaging method was widely adopted in MRgHIFU treatment. With this method, one MR phase image is acquired before the treatment as a reference, and the following MR phase images are acquired during the treatment. By subtracting the following MR phase images from the reference phase image, temperature maps can be computed.

However, this method is significantly biased by the variations of the magnetic field during the treatment due to the movements of the ultrasound applicator. All phase changes in the images are assumed to be from temperature changes. The variations of magnetic field between the reference and temperature scans are translated to errors in the temperature maps. During the MRgHIFU treatment, the ultrasound applicator is moved mechanically so that the ultrasound focus can cover the whole tumour volume for ablation in the case of a single fixed focus applicator and also in the case of a phased array applicator. Due to the difference in magnetic susceptibility of the ultrasound applicator and the surrounding de-gassed water, the local magnetic field will change when the ultrasound applicator moves to different positions. In the conventional PRF shift-based phase mapping method, in order to avoid temperature measurement errors induced by the ultrasound applicator, the reference phase image has to be repetitively acquired when the applicator is moved to a new position. This brings two major problems to the MRgHIFU treatment.

1. To ablate a certain volume of tumour, the ultrasound focus will be moved many times to cover the whole treatment volume, hundreds or even thousands of steps in the case of a large tumour. Since the ultrasound focus is a few mm across the transverse direction, and up to tens of mm in the axial direction, the effective

volume of ultrasound focus is about $100 \sim 500 \text{ mm}^3$ compared to a medium-sized tumour of $\sim 80 \text{ cm}^3$. With each applicator movement the acquisition of a new reference phase image is necessary, resulting in a treatment process that is very complex and time consuming.

2. The ablated region must be fully cooled down before a new reference phase image is acquired. In the PRF shift-based method, the temperature of a reference phase image is assumed to be known, typically 37°C for the human body. If the ablated region is not fully cooled down when a new reference phase image is acquired, the calculated temperature map from the phase difference between the reference and temperature scans will deviate from the real temperature in this region. As the tissue cooling down time may vary from around one minute to several minutes, the total treatment time is quite long. A long treatment time of several hours for large tumours could be clinically unacceptable.

A method of self-reference was proposed by Viola Rieke [18] based on the PRF shift method, in which a reference phase image in the heated region is estimated by polynomial fitting and extrapolating from the non-heated region. By using the self-reference method, temperature measurement errors caused by the inter-scan magnetic field variations can be intrinsically avoided. A good result can be obtained using this method when the tissue structure of the heated region is simple and uniform. However, in a clinical environment, regions to be treated generally show complex structures; often the phase is not continuous in the non-heated region, especially at the boundaries between different tissues, e.g. water and fat, blood vessel, etc. The extrapolated phase image for reference could be completely fault. It is very difficult to obtain an accurate reference image for general cases. The clinical application of the self-reference method is limited to regions inside an organ with uniform tissue [19].

In this paper we propose a method to eliminate temperature measurement errors caused by ultrasound applicator susceptibility. A calculated or pre-measured delta magnetic field induced by the ultrasound applicator is employed to compensate for the field variations due to repositioning of the applicator. The reference image can be repetitively used when the ultrasound applicator changes position, thus reducing the intensively repetitive process of acquiring new reference images. Our proposed method effectively reduces temperature measurement errors, and the treatment workflow of MRgHIFU can be optimised, resulting in a reduction in total treatment time.

Methods

Principle

An MR gradient echo sequence is used to measure phase images for both reference scans and temperature scans. Due to local temperature changes in the tissue, the proton resonance frequency is shifted accordingly, and the frequency changes can be measured in MR phase images. Temperature changes ΔT can be calculated as:

$$\Delta T = \frac{\Delta\phi}{\gamma \cdot B_0 \cdot \alpha \cdot T_E} \quad (1)$$

where γ is the gyromagnetic ratio (2.675×10^8 rad/s/Tesla for protons), B_0 is the main static magnetic field strength, T_E is the echo time, α is a temperature-dependent coefficient, (typically -0.01 ppm/ $^\circ\text{C}$ for tissues [20]), and $\Delta\phi$ is the phase changes between the reference scan and temperature scan.

$$\Delta\phi = \phi_T - \phi_R \quad (2)$$

where the phase image ϕ_R is acquired as a reference before the HIFU heating and ϕ_T is acquired during or after HIFU heating.

The magnetic field of an ideal MRI system is homogeneous with the field strength of B_0 within the imaging volume. Practically, a small inherent inhomogeneous field contribution ΔB_c is present, so the real magnetic field B is also:

$$B(x, y, z) = B_0 + \Delta B_c(x, y, z) \quad (3)$$

In an MRgHIFU environment, due to the magnetic susceptibility difference between the ultrasound applicator and its surrounding de-gassed water, the ultrasound applicator will induce an additional magnetic field ΔB_t superposed on the existing magnetic field. Since there are no non-linear magnetic objects such as ferrous material present in the MRI imaging region, the spatial distribution of the delta magnetic field ΔB_t is constantly relative to the coordinate system fixed on the ultrasound applicator on the condition that the applicator moves only translationally or rotates along B_0 direction. The relationship between the magnet coordination system and the applicator coordination system is shown in Figure 1.

In the case of the ultrasound applicator only moving translationally without rotation, the induced delta magnetic field $\Delta B_{t(\mathbf{r})}(x, y, z)$ for the applicator at position $\mathbf{r}=(a, b, c)$ can be calculated by the translation of $\Delta B_t(x', y', z')$ induced in the ultrasound applicator coordinate system:

$$\Delta B_{t(\mathbf{r})}(x, y, z) = \Delta B_t(x - a, y - b, z - c) \quad (4)$$

In the case of the applicator rotating by θ degrees along the direction of B_0 as well as moving

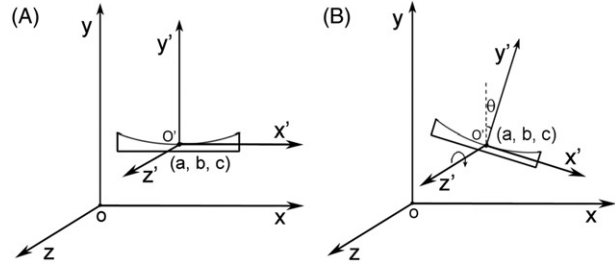


Figure 1. Magnet coordination system xyz and ultrasound applicator coordinate system $x'y'z'$. The direction of the main static magnetic field is in parallel with the z axis. The origin of the ultrasound applicator coordinate system is (a, b, c) in the magnet coordinate system. Relations between the applicator coordination system and the magnet coordination system are: (A) translation, (B) translation and rotation along z direction.

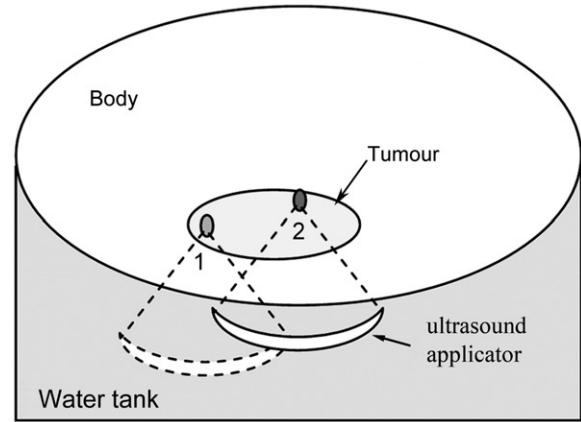


Figure 2. Diagram of tumour treatment by MRgHIFU. After finishing the treatment at position 1, the ultrasound applicator is moved to position 2. The ideal workflow is: a reference image is acquired at position 1 for temperature imaging, when the applicator is shifted to position 2, the reference image can still be used for calculating a temperature map.

translationally to the position $\mathbf{r}=(a, b, c)$, the induced field is:

$$\begin{aligned} \Delta B_{t(\mathbf{r})}(x, y, z) &= \Delta B_t(x', y', z') \\ x' &= x \cos \theta + y \sin \theta - a \\ y' &= -x \sin \theta + y \cos \theta - b \\ z' &= z - c \end{aligned} \quad (5)$$

As in Figure 2, where the ultrasound applicator is at position 1, $\mathbf{r}_1=(x_1, y_1, z_1)$, the magnetic field can be expressed as:

$$B_{r_1}(x, y, z) = B_0 + \Delta B_c(x, y, z) + \Delta B_{t(\mathbf{r}_1)}(x, y, z) \quad (6)$$

Acquisition of a reference MR phase image at this position, and the phase can be expressed as:

$$\phi_R = \gamma \cdot B_{r_1} \cdot T_E \quad (7)$$

Moving the ultrasound applicator to position 2, $\mathbf{r}_2 = (x_2, y_2, z_2)$, as in Figure 2, the magnetic field, changes to:

$$B_{r_2}(x, y, z) = B_0 + \Delta B_c(x, y, z) + \Delta B_{t(r_2)}(x, y, z) \quad (8)$$

At this position the ultrasound applicator transmits energy to ablate the tumour and an MR phase image is acquired. The phase image measured at this position is given by:

$$\varphi_T = \gamma \cdot B_{r_2}(1 + \alpha \cdot \Delta T) \cdot T_E \quad (9)$$

where ΔT is temperature changes in the tissue.

Subtracting Equation 7 from Equation 9, and replacing B_{r_1} and B_{r_2} with Equations 6 and 8, ΔT can be calculated as:

$$\Delta T = \frac{(\varphi_T - \varphi_R)}{\gamma \cdot B_{r_2} \cdot \alpha \cdot T_E} - \frac{\gamma \cdot [\Delta B_{t(r_2)} - \Delta B_{t(r_1)}] \cdot T_E}{\gamma \cdot B_{r_2} \cdot \alpha \cdot T_E} \quad (10)$$

The first term is equivalent to the conventional PRF shift-based phase different mapping method. The second term is the temperature measurement bias due to the magnetic field variations caused by repositioning of the ultrasound applicator.

In practice, B_{r_2} in Equation 10 can be well approximated by B_0 as the inhomogeneous field component ΔB_c and the ultrasound applicator-induced field ΔB_t are both in ppm range. The ΔB_t induced by the ultrasound applicator susceptibility in the background field of B_0 is spatially fixed in the coordinate system attached to the applicator. The effect of the ppm level inhomogeneity of B_0 on ΔB_t is secondary and can be safely neglected. The ΔB_t can either be numerically calculated, or measured in a laboratory setting.

Calculation of the ultrasound applicator-induced delta magnetic field ΔB_t

The ultrasound applicator-induced delta magnetic field ΔB_t can be calculated by the numerical computation method if the geometry structure of the ultrasound applicator is provided and the magnetic susceptibilities of the employed materials are known. In this method, the ultrasound applicator is divided into small volume elements and the magnetic field induced by each small volume element can be approximated as that from a magnetic dipole. The ultrasound applicator-induced field is the sum of the fields from all the elements. The distant magnetic field of a magnetic dipole $\mathbf{m} = \mathbf{M} \times \Delta V$ can be calculated by:

$$\mathbf{B}(\mathbf{r}) = \frac{\mu_0}{4\pi} \left[-\frac{\mathbf{m}}{r^3} + \frac{3(\mathbf{m} \cdot \mathbf{r})\mathbf{r}}{r^5} \right] \quad (11)$$

where μ_0 is permeability of the free space, \mathbf{M} is magnetisation of the small volume element, and $\mathbf{r} = (x, y, z)$ represents the vector from the dipole centre to a field point.

In the case of a clinical MRI system, the uniformity of the B_0 field within the imaging volume is in ppm level and the magnet coordinate system is normally defined with the main static magnetic field B_0 pointing in z -axis direction. The distant field of a magnetic dipole can be calculated by:

$$\begin{aligned} B_x &= \frac{\mu_0 m}{4\pi} \frac{3xz}{(x^2 + y^2 + z^2)^{5/2}} \\ B_y &= \frac{\mu_0 m}{4\pi} \frac{3yz}{(x^2 + y^2 + z^2)^{5/2}} \\ B_z &= \frac{\mu_0 m}{4\pi} \frac{2z^2 - x^2 - y^2}{(x^2 + y^2 + z^2)^{5/2}} \end{aligned} \quad (12)$$

where the dipole's centre is at the origin of the coordinate system.

In an MRgHIFU environment, the ultrasound applicator is submerged in de-gassed water. Thus, the magnetic moment \mathbf{m} is the result of subtracting the magnetic moment of water from the magnetic moment of the applicator material:

$$\mathbf{m} = \mathbf{m}_a - \mathbf{m}_w = (\mathbf{M}_a - \mathbf{M}_w) \times \Delta V \quad (13)$$

Here, \mathbf{m}_a , \mathbf{m}_w are the magnetic moment of a small volume of the applicator material and the de-gassed water respectively. \mathbf{M}_a and \mathbf{M}_w are the magnetisation for the applicator material and water respectively. Let χ_{m_a} and χ_{m_w} represent the magnetic susceptibilities of the small volume of applicator material and the de-gassed water respectively.

For a non-ferromagnetic medium with magnetic susceptibility χ_m , the magnetisation \mathbf{M} can be calculated by:

$$\left. \begin{aligned} \mathbf{M} &= \frac{\mathbf{B}}{\mu_0} - \mathbf{H} \\ \mathbf{B} &= \mu_0(1 + \chi_m)\mathbf{H} \end{aligned} \right\} \Rightarrow \mathbf{M} = \frac{\mathbf{B}}{\mu_0} \left(\frac{\chi_m}{1 + \chi_m} \right) \quad (14)$$

Therefore the magnetic moment \mathbf{m} is:

$$\begin{aligned} \mathbf{m} &= (\mathbf{M}_a - \mathbf{M}_w) \times \Delta V \\ &= \frac{\mathbf{B}}{\mu_0} \left(\frac{\chi_{m_a}}{1 + \chi_{m_a}} - \frac{\chi_{m_w}}{1 + \chi_{m_w}} \right) \times \Delta V \end{aligned} \quad (15)$$

Both χ_{m_a} and χ_{m_w} are much smaller than 1, at the ppm level, so that Equation 15 can be further simplified for calculation as:

$$\mathbf{m} = (\mathbf{M}_a - \mathbf{M}_w) \times \Delta V \approx \frac{\mathbf{B}}{\mu_0} (\chi_{m_a} - \chi_{m_w}) \times \Delta V \quad (16)$$

The ultrasound applicator-induced delta magnetic field can be obtained by summing the induced field components from all the small volume elements. Since the ultrasound applicator-induced

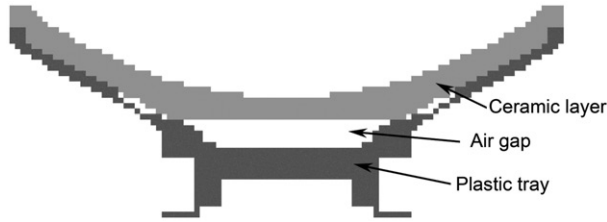


Figure 3. A simplified ultrasound applicator model was used for calculating the delta magnetic field. The model was divided into $2\text{ mm} \times 2\text{ mm} \times 2\text{ mm}$ -sized volume elements. For each volume element we assumed that only one kind of material was contained.

magnetic field is at the ppm level of the main static magnetic field in an MRI environment, the secondary induced field interference between small volume elements can be neglected during the calculation.

A simplified ultrasound applicator model was used for calculating the delta magnetic field; the ultrasound applicator was modelled from a ceramic layer, an air gap and a plastic tray as shown in Figure 3. The size of the applicator model is 180 mm in diameter and 150 mm in focal length. The applicator model was divided into $2\text{ mm} \times 2\text{ mm} \times 2\text{ mm}$ small volume elements. For each small volume element we assume that it is composed entirely of a single material.

Measurement of the ultrasound applicator-induced delta magnetic field ΔB_t

In a static magnetic field, when the ultrasound applicator is placed in a water tank the local magnetic field will change due to the susceptibility difference between the applicator and the water. The variation of the magnetic field ΔB_t can be measured by an MR imaging method. Figure 4 shows a measurement of the delta magnetic field ΔB_t by subtracting the MR phase images acquired with and without the ultrasound applicator in a water tank.

The following steps describe the measurement:

1. A non-magnetic water tank made of plastic is positioned inside the MR scanner. The ultrasound applicator and its supporting frame are put into the water tank. The applicator should be positioned in the same direction as it is in practical use, and the water level is recorded.
2. Acquisition of an MR phase image ϕ_1 with a gradient echo sequence and a fixed parameter setting, e.g. $T_R/T_E = 50\text{ ms}/15\text{ ms}$.
3. While the water tank is kept in the same position inside the magnetic bore, the ultrasound applicator and its supporting frame are taken out from the water tank. Afterwards water is refilled until the water level reaches the same height as recorded in step 1.

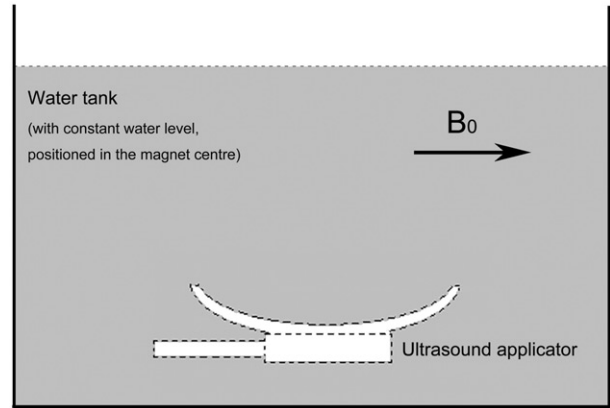


Figure 4. Diagram for measuring the delta magnetic field induced by the ultrasound applicator. A water tank was positioned in the magnet centre. MR phase images were acquired with and without ultrasound applicator in the water tank while keeping the water level constant for both measurements.

4. The same sequence as in step 2 is run with identical parameters to acquire a phase image ϕ_2 .
5. The ultrasound applicator-induced delta magnetic field ΔB_t can be calculated as:

$$\Delta B_t = (\phi_1 - \phi_2) / (\gamma \cdot T_E)$$

Devices

All imaging experiments were performed on a 1.5T superconducting magnetic MRI scanner (MAGNETOM Symphony 1.5T, Siemens Healthcare, Erlangen, Germany). A laboratory custom-built focused ultrasound system was used for the experiments. The system consists of a fixed focus ultrasound applicator (150 mm in focal length, frequency 1.1 MHz and focal size $3\text{ mm} \times 3\text{ mm} \times 15\text{ mm}$), a computer-controlled applicator positioning system and a single channel radio-frequency amplifier system.

Phantom experiment

A 240-mm diameter spherical water phantom was put on the HIFU water tank with a plastic support frame as shown in Figure 5A. No HIFU energy was transmitted during the phantom experiments, therefore any temperature changes shown on the temperature maps could be considered as errors. The ultrasound applicator was shifted along y and z directions at 10 mm intervals respectively. For each movement an MR phase image (gradient echo-based sequence, $T_R/T_E = 50/15\text{ ms}$, field of view (FOV) = 384 mm, slice thickness = 5 mm, pixel size = $2\text{ mm} \times 2\text{ mm}$ and image matrix = 192×192) was acquired for the offline calculation of the temperature maps. The phantom was put into

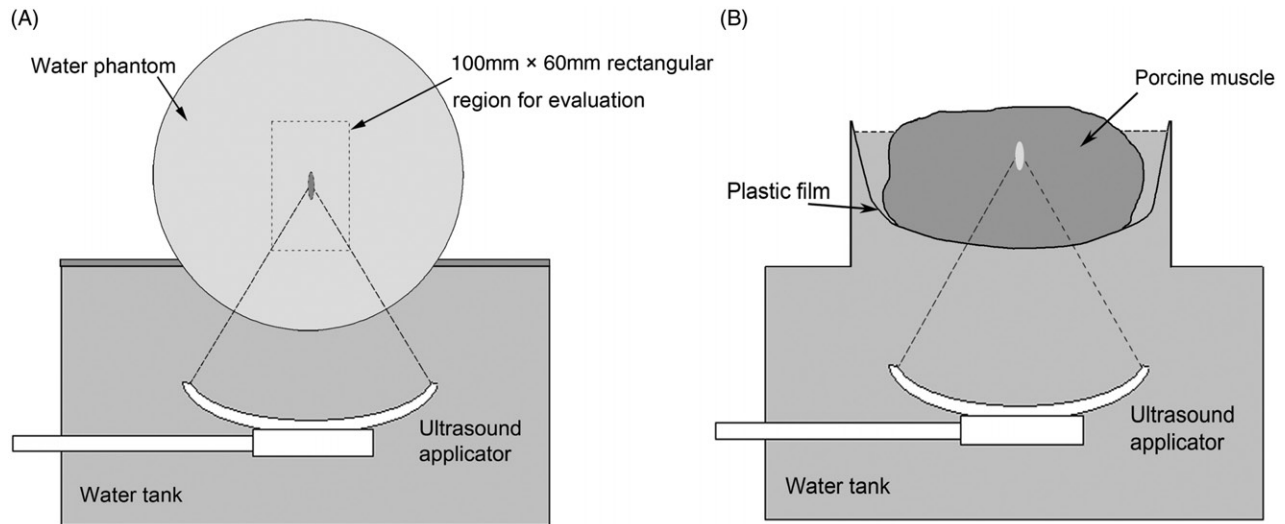


Figure 5. Experimental set-up. (A) Phantom: a 240-mm diameter spherical water phantom was put on the water tank. (B) Ex vivo: a block of porcine muscle was put inside a container with a plastic film beneath it through which ultrasound energy can penetrate freely.

the water tank partially so that the whole acoustic path of the ultrasound applicator could be shown on the images.

A 100 mm \times 60 mm rectangular region of interest, which was centred on the ultrasound focal region, was selected for the image evaluation. To investigate the correlation between the temperature measurement errors and the shifts in the applicator's positions, for each applicator position the following measurements of the distribution of the absolute temperature measurement errors were made – mean, median, maximum and the 95th percentile. We define the applicator free shift range (AFSR) to indicate the ultrasound applicator's maximum shift range in which the 95th percentile of the temperature measurement error is less than 1°C in the rectangular evaluation region. Therefore, the AFSR can directly reflect the capability of the applicator's shift range using the same reference phase image.

Ex vivo experiment

A block of porcine muscle was positioned inside a plastic container suspended from a thin plastic film beneath it as shown in Figure 5B. Acoustic energy can penetrate the plastic film freely. Both the HIFU water tank and the meat container were filled with de-gassed water. An MR phase image was acquired before the HIFU heating as a reference. Then the ultrasound applicator was shifted in the y - z plane to ablate 10 points including the point where the reference image was acquired. The positions of the 10 points were: $(y, z) = (0,0), (0,40), (0,80), (0,20), (0,60), (20,0), (20,40), (20,80), (20,20), (20,60)$, which were relative to the reference position

in mm during a time sequence of HIFU heating. For each applicator position, 400 W of ultrasound power was applied for 2 s to heat the porcine muscle and an MR phase image was acquired to calculate the temperature map. The MR temperature sequence is gradient echo-based with the parameters: $T_R/T_E = 50/15$ ms, FOV = 384 mm, pixel size = 2 mm \times 2 mm, slice thickness = 5 mm, and image matrix = 192 \times 192.

Results and discussion

Ultrasound applicator-induced delta magnetic field

The ultrasound applicator-induced delta magnetic field was measured as shown in Figure 6A with an image plane orientated through the centre of the ultrasound focus. A low pass filter was applied to reduce the image noise. In Figure 6A, on both sides of the ultrasound applicator, black-and-white stripes (discontinuities) can be observed, which can be explained by a large local magnetic field induced near the ultrasound applicator so that the measured phase was wrapped around. These errors do not impact on the practical use as it is located far away from the ultrasound focal region. The calculated applicator-induced delta field is shown in Figure 6B. The field distribution is smoother and noise free compared with the measured field.

Phantom experiment

Without the ultrasound applicator delta magnetic field compensation, the temperature measurement error in a 100 mm \times 60 mm rectangular evaluation

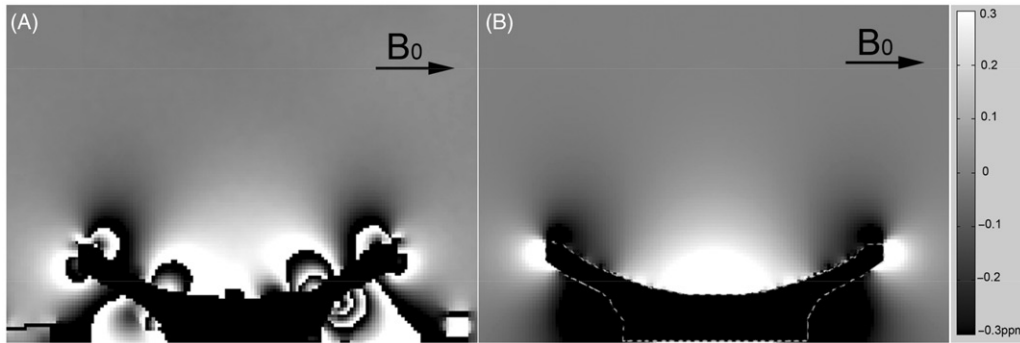


Figure 6. Ultrasound applicator-induced delta magnetic fields. The direction of the static main magnetic field B_0 is indicated by the arrow. The fields are shown (A) from a measurement, (B) by calculation. The magnetic field varies between -0.01 ppm to 0.4 ppm from the focal region to the applicator surface. Phase wraparound can be observed around the applicator due to large magnetic field variations in A; however, it can be neglected during the temperature error compensation as those areas are far away from the ultrasound focal region.

region was increased as the distance of the applicator shifted. This can be observed in both y and z direction as shown in Figures 7 and Figure 8 respectively. The susceptibility bias from the ultrasound applicator was much more pronounced for shifts in the y direction. The corresponding temperature measurement errors increased dramatically with shifts of the applicator in terms of both the affected area of the image and the magnitude of the temperature measurement errors.

In Tables I and II, the mean, median, maximum and the 95th percentile of the absolute temperature measurement errors were calculated for the applicator shift in y and z directions respectively. As shown in Figure 9, without compensating the applicator-induced delta magnetic field, the temperature measurement error at the 95th percentile increased rapidly with the applicator shifting from the reference position, while the temperature measurement error is kept at a moderate value when employing the compensation.

For this ultrasound applicator which was used for the experiments, the AFSR in z direction was 20 mm without compensation and 70 mm with compensation method based on the pre-measured field or calculated field. In y direction, the AFSR is <10 mm without compensation, 20 mm and 50 mm with compensation by pre-measured field and by the calculated field respectively.

Ex vivo experiment

Ex vivo experiments were done with porcine muscle. Because the HIFU heating was performed in a time sequence (1.5 min intervals) for the 10 points, the heat diffused out of the heated points and they were not fully cooled down when the temperature image was acquired for the next HIFU heating. The delta temperature map calculated by the conventional PRF

shift-based method is shown in Figure 10A. Large temperature measurement errors can be found when the applicator was shifted away from the reference position; see the areas indicated by the arrows in Figure 10A.

As can be seen in Figure 10B, the temperature errors were significantly reduced by applying the correction using the pre-measured applicator-induced delta magnetic field. The temperature in the ultrasound focal region and the heated points was shown clearly and accurately. The large temperature measurement errors due to the shifts in the applicator position in Figure 10A were eliminated.

To obtain an accurate temperature map it is important to keep the water level constant when the applicator is shifted from the reference position, otherwise the magnetic susceptibility difference between water and air will induce additional phase offsets that might be misinterpreted as a temperature change around the water–air boundary. In our experimental design, the variation of the water level was controlled within 1 mm when the applicator was moved across the water tank.

By translational shifting or rotating along B_0 direction, the applicator focus can cover most tumours in a clinical treatment. However, in the special case when the applicator doesn't rotate along B_0 direction during HIFU treatment, the spatial distribution of the ultrasound applicator-induced delta magnetic field will change in the applicator coordination system. The new spatial distribution of the applicator-induced delta magnetic field cannot be obtained by simply translating and rotating the pre-measured or calculated delta field. In such a case it is necessary to acquire a new reference image.

In the perspective of using this method in an in vivo setting, continually monitoring temperature for point by point HIFU ablation can be realised

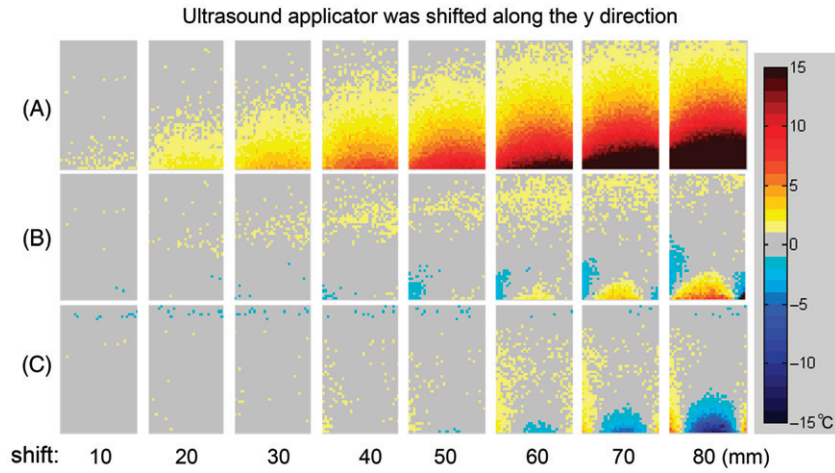


Figure 7. Temperature error map within a 100 mm × 60 mm rectangular evaluation region. The ultrasound focus was located at the centre of the rectangle. The ultrasound applicator was shifted along the y direction. (A) Conventional PRF shift-based method without the applicator delta field compensation. (B) Compensation with the pre-measured applicator delta field. (C) Compensation with the calculated applicator delta field.

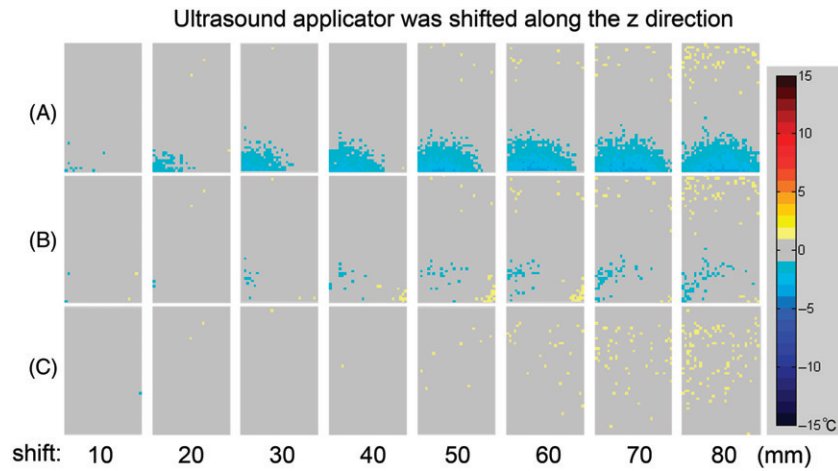


Figure 8. Temperature error map within a 100 mm × 60 mm rectangular evaluation region. The ultrasound focus was located at the centre of the rectangle. The ultrasound applicator was shifted along the z direction. (A) Conventional PRF shift-based method without the applicator delta field compensation. (B) Compensation with the pre-measured applicator delta field. (C) Compensation with the calculated applicator delta field.

Table I. Quantitative temperature error measurement for applicator shifts in y direction.

Shift (mm)	Uncompensated				Compensated with measured field				Compensated with calculated field			
	Mean	Median	P95	Max	Mean	Median	P95	Max	Mean	Median	P95	Max
10	0.42	0.35	1.01	1.61	0.30	0.19	0.71	1.19	0.29	0.17	0.65	1.46
20	0.83	0.68	2.12	2.95	0.40	0.32	0.89	1.43	0.38	0.31	0.76	1.60
30	1.31	0.97	3.50	4.93	0.49	0.38	1.03	1.46	0.41	0.36	0.83	1.34
40	2.09	1.46	5.77	7.90	0.59	0.53	1.23	1.95	0.50	0.48	0.97	1.62
50	2.90	1.89	8.51	11.55	0.56	0.39	1.14	2.93	0.46	0.36	0.95	1.89
60	4.50	3.03	12.55	16.38	0.77	0.70	1.42	2.72	0.70	0.65	1.38	2.50
70	6.19	4.06	17.45	24.07	0.81	0.62	1.66	4.31	0.83	0.55	1.51	5.85
80	8.30	5.41	22.77	33.24	1.01	0.44	3.66	14.40	1.21	0.34	1.48	13.47

Table II. Quantitative temperature error measurement for applicator shifts in z direction.

Shift (mm)	Uncompensated				Compensated with measured field				Compensated with calculated field			
	Mean	Median	P95	Max	Mean	Median	P95	Max	Mean	Median	P95	Max
10	0.25	0.21	0.66	1.41	0.24	0.20	0.58	1.11	0.22	0.19	0.55	1.05
20	0.34	0.27	0.89	1.76	0.29	0.25	0.70	1.22	0.25	0.22	0.61	1.22
30	0.41	0.30	1.37	2.40	0.31	0.27	0.76	1.55	0.24	0.21	0.60	1.12
40	0.46	0.31	1.57	2.86	0.33	0.28	0.79	1.57	0.28	0.26	0.67	1.06
50	0.58	0.38	1.90	3.49	0.38	0.34	0.90	1.63	0.35	0.35	0.81	1.37
60	0.66	0.45	2.21	3.61	0.41	0.36	0.95	1.64	0.39	0.40	0.90	1.40
70	0.71	0.51	2.27	3.79	0.43	0.39	0.96	1.82	0.45	0.48	0.99	1.30
80	0.75	0.54	2.30	3.62	0.47	0.44	1.06	1.77	0.53	0.56	1.12	1.65

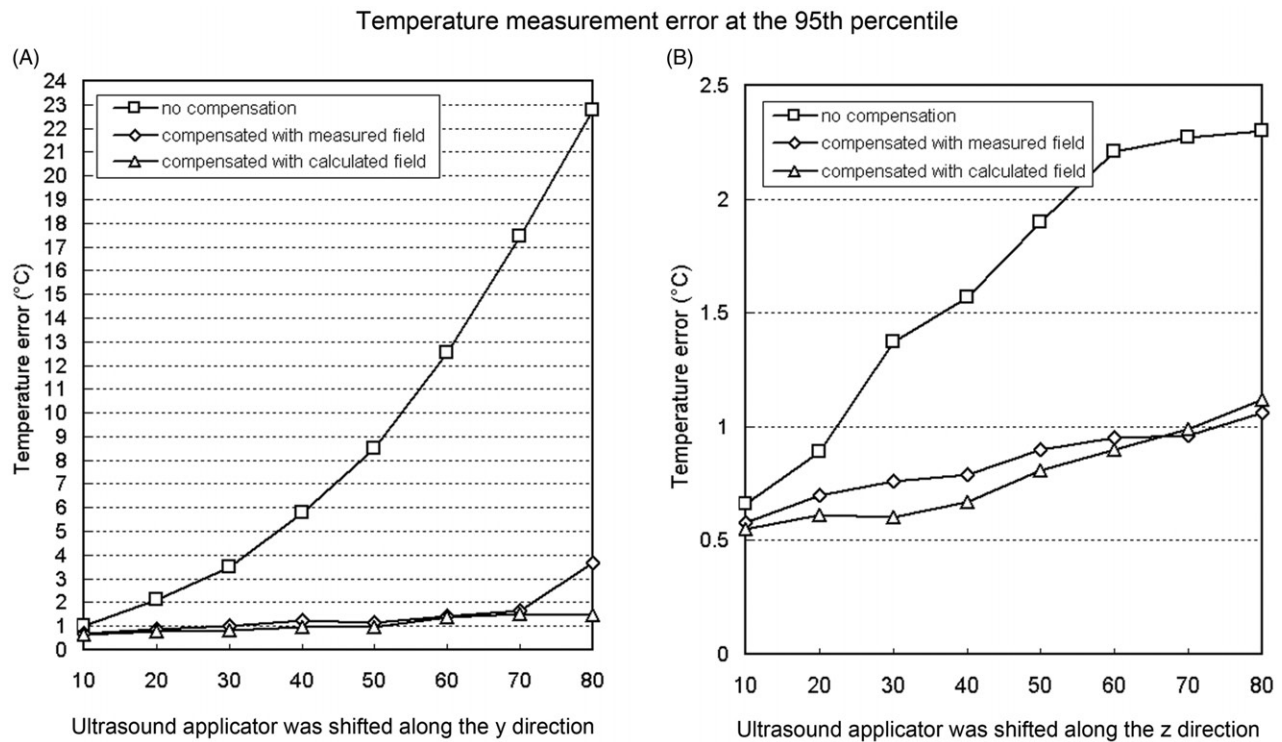


Figure 9. Temperature measurement error at the 95th percentile in the $100\text{ mm} \times 60\text{ mm}$ evaluation region correlated to the distance of the ultrasound applicator from the position where the reference image was acquired. Ultrasound applicator was shifted in (A) y direction and (B) z direction.

without the interruption of repetitively acquiring reference phase images. This can be a big advantage to improve the MRgHIFU workflow. Considering the interference from blood vessels and the interface of tissues, we cannot expect to remove them by this method due to phase information contaminated by these factors. However, the temperature measurement errors are restricted to the blood vessel or tissue interface locally. If the heating point is not located at such a region, the measured temperature is still reliable. Monitoring patient-related movement is necessary to ensure the accuracy of the MR temperature measurement as well as the precise location

of the treatment. The last point to be considered practically is the validity of the pre-measured or the calculated ultrasound applicator-induced magnetic field. The ultrasound applicator-induced magnetic field ΔB_t is kept constant in the ultrasound applicator coordinate system when the applicator is moved within the homogenous region of the magnet. Therefore we expect that the temperature measurement errors induced by the ultrasound applicator susceptibility can be removed. While in the event that the applicator is shifted to the borders of the magnet where the magnetic field inhomogeneities increases, the actual ultrasound applicator-induced delta field

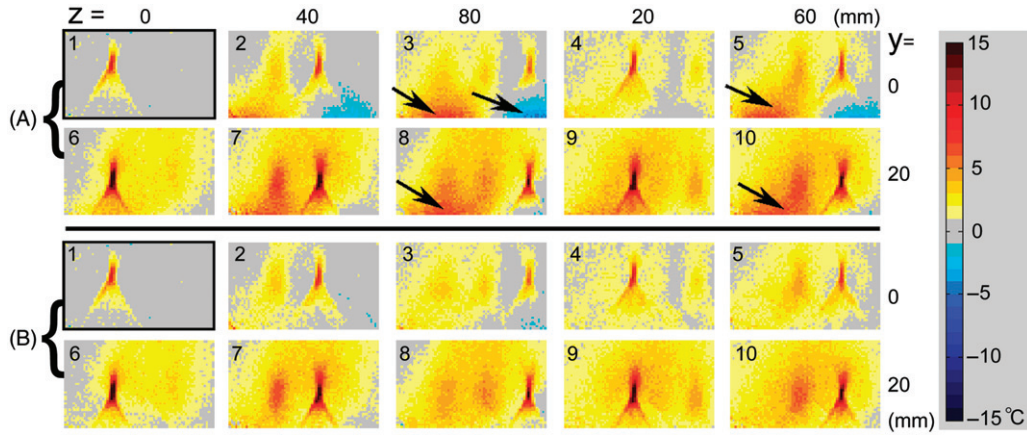


Figure 10. Ex vivo experiments with porcine muscle. Ten ablations were applied at different ultrasound applicator positions. The values of y and z indicate the shifts of the applicator from the position where the reference image was acquired. (A) Delta temperature map without ultrasound applicator delta magnetic field compensation. (B) With ultrasound applicator delta magnetic field compensation. Images were sorted in a time sequence of HIFU heating with labels 1~10. The temperature measurement errors in group A, indicated by arrows, were significantly reduced by compensating the ultrasound applicator-induced delta field in B. The ultrasound foci and the heated region which did not fully cool down during the sequence can be shown clearly and accurately.

will deviate from the pre-measured or the calculated field. In this case the temperature measurement error cannot be completely compensated.

To choose the pre-measured applicator-induced field or the calculated field for practical use, we consider using the calculated field when the inner structure of the applicator and the magnetic susceptibility of applicator materials are precisely known because it gives better accuracy and does not induce additional noise, while usually for a commercial ultrasound applicator, the inner structure and the magnetic susceptibility of applicator materials cannot be precisely obtained, therefore the pre-measured field can be employed. Both the pre-measured field and calculated field are obtained offline, there is no difference regarding the time and complexity when employing them in the temperature monitoring procedure.

Temperature measurement error analysis during MRgHIFU treatment

The major sources of temperature measurement errors when using the PRF shift-based phase mapping method are:

1. Signal-to-noise ratio of the acquired phase images for calculating the temperature map. The noise of an acquired phase image will reduce the temperature accuracy. Optimising the echo time T_E can yield an increased phase-contrast-to-noise ratio, thereby improving the temperature accuracy. The signal-to-noise ratio of the phase difference depending on T_E can be written as:

$$\text{SNR}_{\Delta\phi} \propto T_E \cdot e^{-\frac{T_E}{T_2^*}} \quad (17)$$

The $\text{SNR}_{\Delta\phi}$ can be optimised when T_E equals T_2^* [21].

2. Motion. Moving objects will cause local magnetic field distortions due to susceptibility discontinuities. During an MRgHIFU treatment, the major motions that may affect the temperature accuracy include: (1) movements of the body and of the internal organs of the patient; (2) movement of the ultrasound applicator and its supporting frame; (3) turbulence of water during ultrasound energy transmission; and (4) the fluctuation of the water level. The temperature measurement errors caused by the movement of the ultrasound applicator and its supporting frame can be eliminated by the proposed method. However, reducing the effect of the patient-related movement is a big challenge for MR imaging. With the PRF shift-based phase mapping method, when a movement of the treated region is detected, the reference images must be re-acquired. The effect of water turbulence during ultrasound energy transmission can be neglected if the treated region is far away from the skin which is adjacent to the de-gassed water. When the treated region is very close to the skin, error caused by water turbulence cannot be ignored. A gel pad can be inserted between water and skin to reduce the effect of water turbulence. Precise water level monitoring and controlling can be achieved through proper design of the water tank.
3. Phase wraparound in the ultrasound focal region due to high temperature changes and long echo time T_E . In Equation 1, $\Delta\phi$ will exceed $\pm\pi$ when there are large temperature changes with long echo time T_E . Because the four-quadrant

inverse tangent function is used for phase calculation, the calculated $\Delta\phi$ will be wrapped around into $[-\pi, \pi]$ when temperature variation exceeds the following criterion.

$$|\Delta T| > \frac{\pi}{\gamma \cdot B_0 \cdot \alpha \cdot T_E} \quad (18)$$

A phase unwrapping algorithm needs to be employed to correct this kind of error. Alternatively, phase wraparound errors can be avoided by selecting a shorter echo time in the temperature imaging sequence, e.g. set $T_E = 15.7$ ms or less if $|\Delta T|$ is less than 50°C for a 1.5T scanner; however a shorter T_E will adversely decrease the temperature sensitivity, so that an optimum between temperature sensitivity and phase wrap-around errors must be found.

4. Partial volume effects. In the case of different material components inside a voxel, the MR signal is the averaged contribution from all the materials in that voxel. This is called the partial volume effect. Therefore, the MR temperature map is the averaged temperature in the voxel. In order to catch the highest temperature changes in the ultrasound focal region, the imaging voxel should be set to less than the size of the ultrasound focus.

Treatment time

For the ultrasound applicator which was used in our experiments we made a comparison of total treatment time between the conventional method and our proposed method. A moderate-sized tumour with diameter of 60 mm, volume of 120 cm^3 was assumed for MRgHIFU treatment. 12 slices with approximately 250 heating points were planned for treating the whole tumour volume. Imaging speed was 3 s per slice (for both the reference scan and the temperature scan). Tissue cooling down time was 90 s before a new reference scan. And three continuous temperature measurements were applied to monitor HIFU ablation of one point. Considering the AFSR of 10 mm in y and 20 mm in z direction for the convention method, 60 reference scans are necessary, resulting in a total treatment time of 130 min. This can be reduced to 55 min with 12 reference scans by our proposed method. A calculated ultrasound applicator-induced delta magnetic field with an AFSR of 50 mm in the y and 70 mm in the z direction was used for the calculation. The user operating time is not considered in this calculation.

Conclusion

A method using a calculated or pre-measured delta magnetic field distribution induced by the ultrasound

applicator is proposed to compensate for the temperature measurement errors due to the applicator's susceptibility during an MRgHIFU treatment. By using this method the reference phase image can be repetitively used when the ultrasound applicator is repositioned to treat different sub-regions. Furthermore, the frequency of waiting for the treated tissue to cool down and repetitively acquiring the reference images is significantly reduced. Therefore the complex and time-consuming workflow of MRgHIFU treatment, based on the PRF shift MR temperature mapping, is simplified, resulting in a substantial reduction in total treatment time.

Acknowledgements

The authors wish to thank Chongqing HAIFU(HIFU) Technology for supplying a HIFU system for the experiments. We also gratefully acknowledge help from Adrian J. Boelens in proof-reading this document.

Declaration of interest: The authors report no conflict of interest. The authors alone are responsible for the context and writing of the article.

References

1. Rivens I, Shaw A, Civale J, Morris H. Treatment monitoring and thermometry for therapeutic focused ultrasound. *Int J Hyperthermia* 2007;23:121–139.
2. Kokuryo D, Kaihara T, Kumamoto E, Fujii S, Kuroda K. Method for target tracking in focused ultrasound surgery of liver using magnetic resonance filtered venography. *Conf Proc IEEE Eng Med Biol Soc* 2007;1:2614–2617.
3. Gianfelice D, Gupta C, Kucharczyk W, Bret P, Havill D, Clemons M. Palliative treatment of painful bone metastases with MR imaging-guided focused ultrasound. *Radiology* 2008;249:355–363.
4. Gerard C. Van Rhoon, Peter Wust, Introduction: Non-invasive thermometry for thermotherapy. *Int J hyperthermia* 2005;21:489–495.
5. Kirkham AP, Emberton M, Hoh IM, Illing RO, Freeman AA, Allen C. MR imaging of prostate after treatment with high-intensity focused ultrasound. *Radiology* 2008;246:833–844.
6. Rieke V, Kinsey AM, Ross AB, Nau WH, Diederich CJ, Sommer G, Pauly KB. Referenceless MR thermometry for monitoring thermal ablation in the prostate. *IEEE Trans Med Imaging* 2007;26:813–821.
7. Hynynen K, Clement G. Clinical applications of focused ultrasound – The brain. *Int J Hyperthermia* 2007;23:193–202.
8. Hynynena K, McDannolda N, Clementa G, Jolesza FA, Zadicariob E, Killianyc R, Moorec T, Rosenc D. Pre-clinical testing of a phased array ultrasound system for MRI-guided noninvasive surgery of the brain – A primate study. *Eur J Radiol* 2006;59:149–156.
9. Haar GT, Coussios C. High intensity focused ultrasound: Physical principles and devices. *Int J Hyperthermia* 2007;23:89–104.
10. Haar GT, Coussios C. High intensity focused ultrasound: Past, present and future. *Int J Hyperthermia* 2007;23:85–87.

11. Hynynen K, McDannold N. MRI guided and monitored focused ultrasound thermal ablation methods: A review of progress. *Int J Hyperthermia* 2004;20:725–737.
12. Sapareto SA, Dewey WC. Thermal dose determination in cancer therapy. *Int J Radiat Oncol Biol Phys* 1984;10:787–800.
13. McDannold NJ, King RL, Jolesz FA, Hynynen KH. Usefulness of MR imaging-derived thermometry and dosimetry in determining the threshold for tissue damage induced by thermal surgery in rabbits. *Radiology* 2000;216:517–523.
14. McDannold N, Tempny CM, Fennessy FM, So MJ, Rybicki FJ, Stewart EA, Jolesz FA, Hynynen K. Uterine leiomyomas: MR imaging-based thermometry and thermal dosimetry during focused ultrasound thermal ablation. *Radiology* 2006;240:263–272.
15. Quesson B, de Zwart JA, Moonen CT. Magnetic resonance temperature imaging for guidance of thermotherapy. *J Magn Res Imaging* 2000;12:525–533.
16. Hindman J. Proton resonance shift of water in the gas and liquid states. *J Chem Phys* 1966;44:4582–4592.
17. Ishihara Y, Calderon A, Watanabe H, Mori K, Okamoto K, Suzuki Y, Sato K, Kuroda K, Nakagawa N, Tsutsumi S. A precise and fast temperature mapping method using water proton chemical shift. In: *Proceedings of the SMRM 11th Annual Meeting, Berlin, August 8–14; (1992)*. p. 4803.
18. Rieke V, Vigen KK, Sommer G, Daniel BL, Pauly JM, Butts K. Referenceless PRF shift thermometry. *Magn Reson Med* 2004;51:1223–1231.
19. de Senneville B, Quesson B, Moonen CTW. Magnetic resonance temperature imaging. *Int J Hyperthermia* 2005;21:515–531.
20. McDannold N. Quantitative MRI-based temperature mapping based on the proton resonant frequency shift: Review of validation studies. *Int J Hyperthermia* 2005;21:533–546.
21. Rieke V, Butts K. MR Thermometry. *J Magn Reson Imaging* 2008;27:376–390.